PCCP

Accepted Manuscript

This is an *Accepted Manuscript*, which has been through the Royal Society of Chemistry peer review process and has been accepted for publication.

Accepted Manuscripts are published online shortly after acceptance, before technical editing, formatting and proof reading. Using this free service, authors can make their results available to the community, in citable form, before we publish the edited article. We will replace this *Accepted Manuscript* with the edited and formatted *Advance Article* as soon as it is available.

You can find more information about *Accepted Manuscripts* in the Information for Authors.

Please note that technical editing may introduce minor changes to the text and/or graphics, which may alter content. The journal's standard Terms & Conditions and the Ethical guidelines still apply. In no event shall the Royal Society of Chemistry be held responsible for any errors or omissions in this *Accepted Manuscript* or any consequences arising from the use of any information it contains.

ROYAL SOCIETY OF CHEMISTRY

www.rsc.org/pccp

Journal Name

ARTICLE TYPE

Cite this: DOI: 10.1039/xxxxxxxxxx

Photosynthetic Diode: Electron Transport Rectification by Wetting the Quinone Cofactor†

Daniel R. Martin[a] and Dmitry V. Matyushov*[b‡]

Received Date
Accepted Date

DOI: 10.1039/xxxxxxxxxx

www.rsc.org/journalname

We report 11 μs of molecular dynamics simulations of the electron-transfer reaction between primary and secondary quinone cofactors in the bacterial reaction center. The main question addressed here is the mechanistic reason for unidirectional electron transfer between chemically identical cofactors. We find that electron is trapped at the secondary quinone by wetting of the protein pocket following electron transfer on the time-scale shorter than the backward transition. This mechanism provides effective rectification of the electron transport, making the reaction center a molecular diode operating by cyclic charge-induced electrowetting.

Reaction centers of bacterial photosynthesis convert the energy of light stored in the light-collecting antenna into the transport of electrons across the cellular membrane.[1,2] The transfer of each individual electron occurs as a sequence of underbarrier tunneling transitions between photosynthetic cofactors inserted into the protein complex.[3] The first three hops occur within 200 ps after the absorption of the photon by the primary pair.[4] These reactions proceed with nearly no activation barrier, and they bring the electron to ubiquinone Q_{10} (*Rhodobacter spheroides*) called the primary quinone Q_A. The last and rate-determining step of the electron-transfer chain is from the reduced ubiquinone Q_A^- to the chemically identical secondary quinone Q_B:

$$Q_A^- Q_B \rightarrow Q_A Q_B^- . \qquad (1)$$

The same sequence of electron hops is generated by the second photon. This two-photon process results in absorption of two protons from the cytoplasm, ultimately converting the secondary quinone into quinol Q_BH_2.

The apparent rate of the forward reaction in eqn (1) is $k_{AB} \simeq 10^4$ s^{-1}. It was shown to reflect a complex biphasic kinetics involving a faster component, $k_1 \simeq 10^5$ s^{-1}, depending on the redox potential of Q_A, and a slower component, $k_2 \simeq 10^4$ s^{-1}, independent of the donor's redox potential.[5] It was therefore suggested[6] that conformational gating, involving either a protein conformational change or the movement of the secondary quinone (or both), determines the overall decay of the population of Q_A^-. The fast component in this picture is the actual electron-transfer kinetics reflecting the decay of the "active-state" population following the arrival of the electron to Q_A.

The Q_B^- anion is very stable, but it needs to be protonated before being reduced by the second electron arriving from Q_A^- after the second photon flash.[7] The protonated state Q_BH is about 180 meV higher in the free energy than Q_B^- and its equilibrium fraction is $\simeq 10^{-3}$ relative to the concentration of Q_B^-. Most of Q_B^- is, therefore, present in the anionic form and is also relatively mobile. In contrast, Q_A does not accept a proton, is more restricted for water access, and is tightly bound in its pocket.[8]

The relative stability of the Q_B^- anion poses the question of why the backward recombination reaction, from right to left in eqn (1), does not occur. Indeed, the rate of the second reduction, $\simeq 10^3$ s^{-1}, of Q_BH to form Q_BH^- is significantly slower than the rate of the electron transfer step $k_1 \simeq 10^5$ s^{-1}. Given that Q_A and Q_B are chemically identical, the rates of the forward and backward reactions should be close in the magnitude. The reported value of the reaction Gibbs energy of the forward reaction, $\simeq -60$ meV,[5] would result in the backward rate only an order of magnitude slower than the forward rate, and still much faster than the rate of the second electron transfer. In other words, the last step of the electron transport chain in the reaction center effectively acts as a molecular rectifier, allowing electronic transport in one direction only, despite the mechanistic design based on equal redox components. The potential flaw of such a design was recognized already by Aviram and Ratner in 1974, who used different fragments (one of them quinone) in the proposed molecular rectifier.[9] Resolving the puzzle of the rectifying ability of reaction (1) is a goal of this communication. One can anticipate that the

[a] *Department of Physics, Arizona State University, PO Box 871504, Tempe, Arizona 85287*

[b] *Department of Physics and Department of Chemistry & Biochemistry, Arizona State University, PO Box 871504, Tempe, AZ 85287-1504; E-mail: dmitrym@asu.edu*

† Electronic Supplementary Information (ESI) available: simulation protocol and data analysis. See DOI: 10.1039/b000000x/

Physical Chemistry Chemical Physics Accepted Manuscript

protein surrounding the quinone cofactors creates the asymmetry.[10–12] While this asymmetry does exist, we find that an alternative factor is much more significant: *Wetting of the Q_B^- pocket following the transfer of the negative charge is the main driving force preventing back electron transfer*. Providing this answer has required extensive simulations. Our conclusions are based on the overall 11.5 μs of atomistic molecular dynamics (MD) simulations of the membrane-bound reaction center of *Rhodobacter spheroides* bacterium.

Understanding the factors affecting the activation barrier and free energy of reaction (1) also requires critical re-examining of the basic assumptions of the theory of electron transfer when applied to hydrated proteins as reacting media.[13] The commonly adopted mechanistic picture is based on the combination of geometric and energetic arguments. The geometric argument limits the distance r_{AB} between the donor and acceptor through the well-established exponential decay of the electron tunneling probability.[14] The energetic arguments are based on the Marcus bell-shaped energy gap law establishing a quadratic dependence of the activation barrier on the reaction free energy ΔF_0.[15,16] The reorganization energy of electron transfer λ quantifies in this picture both the driving force ($-\Delta F_0$) required to achieve zero activation barrier and the curvature of the inverted parabola. This picture anticipates optimization of protein electron transfer for energy production in terms of r_{AB} and ΔF_0. This philosophy is in full display in the Dutton parametrization,[17] which assumes nearly constant value of the reorganization energy $\lambda \simeq 0.8$ eV and leaves r_{AB} and ΔF_0 to vary, in limited ranges, among different reactions.

The assumption of a constant and relatively low reorganization energy does not agree with available data from computer simulations.[13,18–20] More generally, the idea of a low-polarizable protein continuum, producing a low reorganization energy, disregards low-frequency, high-amplitude fluctuations of the protein altering the positions of partial charges at molecular groups and ionized residues.[21] The non-polarizable, low-polarity protein fits well the paradigm of the frozen structure advocated by low-temperature X-ray crystallography. However, a room-temperature hydrated protein is an elastically mobile polymer characterized by a broad range of local and global structural relaxation processes.[21] These elastic motions make the protein-water interface a source of intense electrostatic noise, a fluctuation machine, producing corresponding large-scale fluctuations of the energy levels of electrons localized on redox cofactors. Combining the high amplitude of electrostatic fluctuations with their dispersive dynamics (many relaxation times) brings about a physical picture that requires a paradigm shift in the theoretical description of electron-transfer reactions.[13,18]

The complex dynamics of the protein-water interface requires paying attention to the magnitude of the reaction time τ_r relative to the relaxation times of the bath modes affecting the donor-acceptor energy gap (the reaction coordinate[13]). When the reaction time falls shorter than some of the bath relaxation times, the corresponding modes become dynamically frozen on the reaction time-scale and do not contribute to the activation barrier. This is particularly true for the conformational transitions of proteins taking place on the time-scale of milliseconds or longer and in many cases slower than ns-μs times of electronic transitions. The physical consequence of this separation of time-scales is that many electron-transfer reactions occur in conformationally quenched proteins, unable to explore the entire phase space of conformations consistent with a given redox state.

This general phenomenon is known in the field of glass science as ergodicity breaking. It is known to invalidate the fluctuation-dissipation theorem establishing, in its static limit, a connection between the first and the second moments of statistical variables.[22] In the context of electron transfer, ergodicity breaking results in the separation between the parameters defining the average donor-acceptor energy gap (considered as the reaction coordinate[3]) and the curvature of the Marcus parabola. If one starts with the reorganization energy λ as the curvature parameter, the standard formulation[15,16] then dictates that the average energy gap $\langle X\rangle_i$ in the initial ($i=1$) and final ($i=2$) states are expressed in terms of λ and ΔF_0: $\langle X\rangle_i = \Delta F_0 \pm \lambda$, where "+" refers to $i=1$ and "−" refers to $i=2$. In contrast to this simple and well-established result, nonergodic electron transfer requires[13,23] $\langle X\rangle_i = \kappa_G \Delta F_0 \pm \lambda^{St}$, where $\kappa_G = \lambda/\lambda^{St}$. Here, one has to specify an additional energetic parameter, the "Stokes shift reorganization energy" λ^{St}. Similarly to the Stokes shift in spectroscopy, it defines the difference in the vertical transition energies, i.e., the difference in the positions of parabolas' minima, $2\lambda^{St} = \langle X\rangle_1 - \langle X\rangle_2$, plotted against the energy-gap reaction coordinate X.[3] The resulting model for the activation barrier requires three parameters, instead of two parameters, λ and ΔF_0, of the Marcus model. Non-parabolic free energy surfaces would bring more parameters to the model, but such extensions require enhanced sampling[24] still too costly for large protein complexes.

The introduction of the third parameter in the two-parameter Marcus model of electron-transfer[15] opens more flexibility in controlling the activation barrier and allows lower barriers without requiring strongly exergonic reactions. The mechanistic condition for this kinetic improvement is $\kappa_G \gg 1$, as indeed found in many simulations of protein electron transfer.[13,18] In our present, longest so far, simulations of the bacterial reaction center we find the same phenomenology for reaction (1): the reorganization energies extracted from the variance of the energy gap (curvature of the Marcus parabola) is significantly higher than the commonly assumed "universal" values, but $\kappa_G > 1$ keeps the barrier low. While this phenomenology allows us to reproduce the observed forward rate, it does not resolve the problem of unidirectional electron transport. The microscopic picture of wetting of the quinone pocket needs to be involved to fully understand this important reaction.

As mentioned above, the secondary quinone is significantly more mobile than the primary quinone.[8] Two sites of Q_B, the distal and proximal, both in respect to the non-heme iron, were identified by X-ray crystallography[25] (Fig. 1). The distal site is known to be inactive for electron transfer, while most studies indicate that quinone in the proximal site is involved in electron transfer.[26] Consistent with the standard picture, the proximal site is ~ 250 meV more exergonic than the distal site and ~ 5 Å closer to Q_A. It has been therefore suggested[27] that these two factors,

Physical Chemistry Chemical Physics Accepted Manuscript

This journal is © The Royal Society of Chemistry [year]

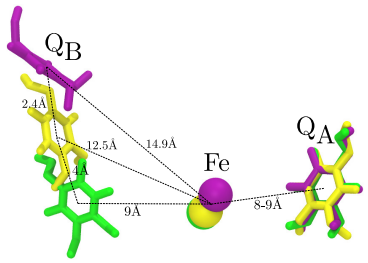

Fig. 1 Schematic representation of positions of the primary, Q_A, and secondary, Q_B, quinones in the reaction center of *Rhodobacter sphaeroides*. The configurations shown are obtained from MD simulations of the distal site (magenta), the intermediate site to which Q_B^- travels within 2 μs of the simulation trajectory (yellow), and the position of the quinone cofactors in the proximal configuration (green). Also shown is the non-heme iron carrying the charge $+2$ in the simulations. All distances are in Å and are between the centers of the corresponding cofactors.

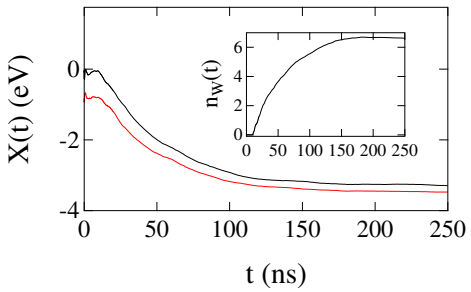

Fig. 2 Time-dependent change of the donor-acceptor energy gap produced by all water molecules in the simulation cell (black). Also shown is the changes in the interaction energy of Q_B^- with water (red). The inset shows the alteration of the number of water molecules in the first hydration layer of Q_B^- following the reduction by Q_A^-.

the higher tunneling probability and a more downhill reaction free energy, are the key mechanistic parameters making Q_B active in the proximal site.

The relative occupancy of the distal and proximal sites by Q_B is not well established since it varies widely between different reported crystal structures.[12] In contrast, the anion Q_B^- is always found in the proximal site. Since the movement of Q_B to the proximal site is often considered to be the prerequisite to electron transfer, it is useful to compare the electron transfer rates in both sites. We therefore performed a number of simulations starting with Q_B in the distal site (details of the simulation protocol can be found in the ESI†). The simulation trajectory 9 μs long of the $Q_A^-Q_B$ with distal Q_B was produced on the Anton supercomputer.[28] This trajectory followed by ~ 2.5 μs simulations of the reduced $Q_AQ_B^-$ state. We have found from this simulation that Q_B^- indeed starts to shift toward the proximal position upon gaining the negative charge (yellow in Fig. 1), consistent with previous simulations.[29] However, it could not reach its final destination at the proximal position (green in Fig. 1) because of either the limited simulation time or an activation barrier separating the two sites.

The second simulation trajectory also revealed the importance of hydration water at the Q_B site in the energetics of electron transfer. We found that the average number of hydration waters n_w in the quinone's first hydration layer (3 Å thick) increased from nearly none, $n_w \simeq 0.25$, in the neutral state to a significantly larger number, $n_w \simeq 5$, in the anionic state. Even more importantly, the donor-acceptor energy gap $X(t)$ between the electronic states of Q_A and Q_B^- (see ESI† for a detailed definition) has drifted in parallel with the increasing level of Q_B^- hydration to a significantly more negative value recorded at the end of the simulation trajectory. The time-scale of the wetting process is about ~ 100 ns (Fig. 2). In order to understand what does it mean for the theory of reaction rates, one has to turn to the physical principles of electron transfer activated by nuclear modes of the thermal bath.

The conceptual foundation of the Marcus theory of electron transfer is the idea, well supported by simulations,[3,30] that the statistics of the fluctuating variable of the donor-acceptor energy gap X is Gaussian. The corresponding free energy surfaces along the reaction coordinate are given by parabolas: $F_i(X) = F_{0i} + (X - \langle X\rangle_i)^2/(4\lambda)$, where the reorganization energy λ defines the parabolas' curvature and $\langle X\rangle_i$, as defined above, are the average gaps in the initial and final states. As mentioned above, the connection between $\langle X\rangle_i$ and the reaction free energy changes from the Marcus theory when nonergodicity is introduced. However, the chemical identity of the two cofactors significantly simplifies the problem. The average donor-acceptor gap is the sum of the gas-phase part X_0 and the solvent-induced part X_s. The former is zero due to the chemical identity of the cofactors. The activation energy of electron transfer becomes particularly simple in this case

$$F_i^{\rm act} = \frac{(X_{si})^2}{4\lambda} \tag{2}$$

and the reaction free energy becomes

$$\Delta F_0 = (X_{s1}^2 - X_{s2}^2)/(4\lambda). \tag{3}$$

All parameters in these equations are available from simulations. The reorganization energy is taken from the variance of the energy gap[13]

$$\lambda = \langle(\delta X)^2\rangle/(2k_{\rm B}T), \tag{4}$$

where $\delta X = X - X_{si}$. The calculation of the rate is completed by using the non-adiabatic Levich-Marcus expression[16]

$$k_i = \frac{V_{\rm AB}^2}{\hbar}\left(\frac{\pi}{k_{\rm B}T\lambda}\right)^{1/2} \exp\left[-F_i^{\rm act}/(k_{\rm B}T)\right]. \tag{5}$$

Equation 5 contains the electron-transfer matrix element $V_{\rm AB}$ representing electron tunneling between Q_A and Q_B.[16] Several calculations of this parameter have been reported.[31–33] Other estimates[5] are based on Dutton's rule[17] and the spin exchange interaction measured by ESR.[34] The values of $V_{\rm AB}$ from these studies are: 0.8×10^{-4} eV,[5] 3×10^{-4} eV,[34] 3.5×10^{-4} eV for superexchange ET and 4.5×10^{-7} eV for direct tunneling.[32] In addition, $V_{\rm AB}$ between menaquinone at Q_A site and ubiquinone at Q_B site are: 1.3×10^{-5} eV[31] (*Rhodopseudomonas viridis*) and 1.7×10^{-4} eV[33] (*Blastochloris viridis*). The data from most recent calculations all reasonably agree with the experimental es-

Physical Chemistry Chemical Physics Accepted Manuscript

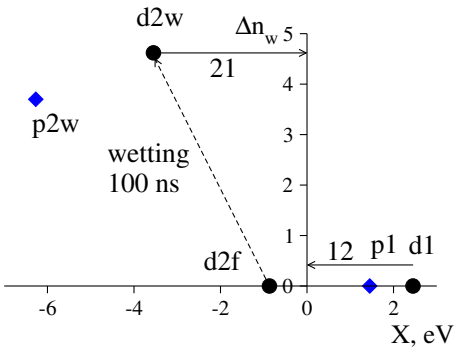

Fig. 3 Schematic representation of electron transfer in reaction (1) in the space of the polarization reaction coordinate X and wetting of the secondary quinone given as the change of the number of waters in its first hydration layer Δn_w. The points represent average configurations $(X_s/\mathrm{eV}, \langle \Delta n_w \rangle)$: p1 $= (1.45, 0)$, d1 $= (2.45, 0)$, d2w $= (-3.55, 4.62)$, p2w $= (-6.3, 3.7)$. The black circles refer to the distal site (d) and the blue diamonds correspond to the proximal site (p); "w" represents wet secondary quinone, "f" is used to indicate artificially frozen water translations in MD simulations. Forward electron transfer (12) proceeds from X_{s1} to the activated state at $X = 0$ along the reaction coordinate X corresponding to dry Q_B. Wetting of the anion Q_B^- follows electron transfer on the time-scale of ~ 100 ns (dashed line). The result of wetting is a significant increase in the magnitude of X_{s2}, which makes the barrier of the backward reaction (21) much higher (eqn (2)). This mechanism achieves the rectification of electron transport in the direction from the primary to the secondary quinone.

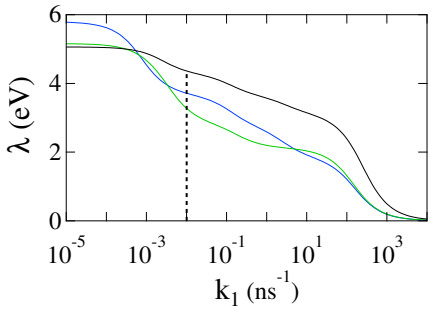

Fig. 4 Nonergodic reorganization energy $\lambda(k)$ (black) observed on the reaction time $\tau_r = k_1^{-1}$ calculated from the 9 μs simulation trajectory of the distal Q_B site (Table 1). Also shown are the protein (green) and water (blue) components of the reorganization energy. They do not add up to the total λ because of cross, water-protein, correlations (see ESI† for more detail). The dashed vertical line indicates the length of the simulation trajectory used in the simulations of the proximal site.

timate,[34] $V_{AB} = 3 \times 10^{-4}$ eV, adopted in our calculations. This V_{AB} refers to proximal Q_B. The exponential decay correction[17] $V_{AB}(r) \propto \exp[-\gamma r]$ with $\gamma = 0.7$ Å^{-1} was used for the distal site.

To apply eqns (2) and (5), one has to be careful about specifying the initial and final states of electron transfer. The standard formulation of the electron transfer theory assumes that the medium reorganization does not involve any major structural or conformational changes. If they occur, a separate reaction coordinate specifying such conformational changes is required. This is indeed the difficulty with defining the nuclear modes coupled to the electron localized on the secondary quinone. The alteration of the hydration environment, which occurs on a relatively long time scale of ~ 100 ns and cause the drift of the energy gap by ~ 3 eV (Fig. 2), needs to be recognized as a separate reaction coordinate, or nuclear mode, coupled to electron transfer. We therefore offer a picture involving wetting as a separate coordinate specifying the state of the system.

In order to separate wetting from polarization fluctuations of the water-protein bath, we have performed a separate simulation of the $Q_B^- Q_A$ configuration in which waters in the simulation box were constrained from translations with a harmonic force, thus prohibiting changes in the wetting of Q_B^-, but allowing waters to adjust their orientations. In addition, since Q_B is mobile, both Q_A and Q_B were harmonically restrained in their average positions of the $Q_A^- Q_B$ configuration. This simulation produces a much less negative X_{s2} compared to the unrestricted 2 μs simulation of $Q_B^- Q_A$ (Table 1). The qualitative picture produced by these separate simulation trajectories is summarized in Fig. 3, where the wetting coordinate is specified by the change of the number of waters Δn_w in the first hydration layer of Q_B^- compared to Q_B.

Table 1 presents the reaction times calculated according to eqns (2) and (5) from the activation parameters produced by MD simulations. As is clearly seen, the wetting of Q_B^- affectively traps the electron on the secondary quinone on the time-scale of ~ 100 ns, which is much shorter than the time of the backward transition. The reported rates are also consistent with experiment, despite the fact that the activation parameters and the overall phenomenology significantly deviate from the commonly assumed Marcus picture. We also confirm that the forward rates to the distal site is too slow compared to observations[5,6] due to the combination of a larger donor-acceptor distance (21.5 Å compared to 17.5 Å in the proximal site, Fig. 1) and a higher activation barrier. The results show that trapping of the Q_B^- redox state by wetting is particularly efficient in the proximal state; there is no need for it in the distal site since electron transfer is already too slow. Still, much of the wetting-induced shift of the average energy gap is eliminated when water is prohibited from moving into the pocket by constraining its translations (last line in Table 1).

A note on the reorganization energy is relevant here. The estimates of the rate constant are made with the reorganization energy λ calculated according to eqn (4) from simulations of the proximal site with the MD trajectory close in length to the reaction time τ_r (Table 1). The ability of such simulations to produce sufficient sampling might be in question here. However, the calculation of the reorganization energy from the ~ 9 μs Anton trajectory shows that λ from 0.1 μs simulation is fairly close to λ obtained from the entire trajectory (Fig. 4, see ESI† for more detail). Further, the value of λ corresponding to the reaction time (dashed line in Fig. 4) falls close to the magnitude reported in Table 1. The uncertainties in the calculated $\tau_r \sim 0.1$ μs compared to the experimental value $\tau_r \sim 5-10$ μs are within possible errors of estimating V_{AB} listed above. We also note that eqn (3) allows one to calculate X_{s2} assuming that no trapping of the final state by wetting has occurred and using $\Delta F_0 = -60$ meV as input. Those numbers are listed in the brackets in Table 1. If these numbers are used to represent the statistics of the polarization coordinate X, one arrives at $\kappa_G = \lambda/\lambda^{\mathrm{St}} \simeq 3$ typically found in simulations of protein electron transfer.[13] This anticipated phenomenology is

Physical Chemistry Chemical Physics Accepted Manuscript

This journal is © The Royal Society of Chemistry [year]

Table 1 Average energy gap X_s and the reorganization energy λ (eV) produced by MD simulations. The labeling of electron transfer states is according to Fig. 3.

Reaction	State	X_s	λ	$F^{\mathrm{act,a}}$	$\tau_r/\mu s^b$	$t_{\mathrm{sim}}/\mu s^c$
$Q_A^- Q_B$	p1	1.5	4.5	0.1	0.1	0.1
$Q_A Q_B^-$	p2w[d]	$-6.3(-1.8^e)$	5.4	2.0		0.1
$Q_A^- Q_B$	d1	2.5	5.1	0.2	1050	9
$Q_A Q_B^-$	d2w	$-3.6(-2.8^e)$	10.2	0.4	4.8×10^6	2
$Q_A Q_B^-$	d2f[f]	-0.9	1.7			0.05

[a] F^{act} is the activation energy (eV) of the forward reaction from eqn (1) with $\lambda = (\lambda_{12}+\lambda_{21})/2$ and reorganization energies according to eqn (4) for the forward (12) and backward (21) transitions. [b] $\tau_r = k_1^{-1}$ is the reaction time (eqn (5)). [c] t_{sim} is the length of the simulation trajectory. [d] the backward rate is essentially zero and is not reported. [e] average energy gap calculated from eqn (3) assuming no wetting and $\Delta F_0 = -60$ meV. [f] distal site with water translations frozen in MD simulations.

significantly altered by the charge-induced wetting of the quinone pocket, bringing the final redox state into a new configuration along the wetting reaction coordinate (Fig. 3).

The wetting mechanism of the electron-transfer cofactor discussed here may be a special case of a general design strategy to rectify the electron current in biological energy chains. This mechanism is likely to be employed by signaling proteins as well.[35] Confined water in general and protein cavities in particular are widely spread in molecular biology.[36,37] Many cavities in proteins exist on the brink of wetting/dewetting stability,[38] and the alteration of the charge state of a cofactor inside such a cavity can promote the wetting/dewetting transition. Wetting of a charged cofactor traps the corresponding electronic state, thus preventing the backward reaction (Fig. 3). Such trapping of the intermediate state is required for relatively slow reactions to prevent the backward transition, which is the case of the reaction considered here. For fast reactions, the dynamic freezing of the nuclear thermal bath[13] or a quick alteration of the cofactor's protonation state are alternative design principles preventing the formation of the solvation trap and allowing a fast charge flow in the chain. The latter approach is realized with the Y_Z tyrosine in the water-oxidizing complex of photosystem II.[39]

The similarity between the action of natural enzymes and of electronic circuits designed for computational information processing has been noticed in the past.[40] Enzymes drain the chemical potentials from the surrounding medium to drive specific reactions. The relevant reduction of entropy is equivalent to creating the information content, with a strong analogy to the performance of a computational unit.[41] To secure such information processing, the principle operation of a diode, allowing unidirectional electrical current, needs to be built into an electron transport enzyme. The bacterial reaction center is a central unit of the bacterial "computer". We find here that the microscopic mechanism involving water pumping in a protein cavity, controlled by the electrical charge, is the design principle behind its diode action. This is a general phenomenon of electrowetting[42] utilized in an ingenious design of the natural diode.

Acknowledgement. This research was supported by the NSF (MCB-1157788 and CHE-1464810) and through XSEDE (TG-MCB080116N). Anton computer time (D. E. Shaw Research) was provided by the Pittsburgh Supercomputing Center through Grant P41GM103712-S1 from the NIH.

References

1 D. G. Nicholls and S. J. Ferguson, *Bioenergetics 3*, Academic Press, London, 2002.
2 R. E. Blankenship, *Molecular Mechanisms of Photosynthesis*, Blackwell Science, Williston, VT, 2003.
3 A. Warshel and W. W. Parson, *Ann. Rev. Phys. Chem.*, 1991, **42**, 279–309.
4 W. Zinth and J. Wachtveitl, *ChemPhysChem*, 2005, **6**, 871–880.
5 J. Li, E. Takahashi and M. R. Gunner, *Biochemistry*, 2000, **39**, 7445–7454.
6 M. S. Graige, G. Feher and M. Y. Okamura, *Proc. Natl. Acad. Sci. USA*, 1998, **95**, 11679–11684.
7 M. Y. Okamura, M. L. Paddock, M. S. Graige and G. Feher, *Biochimica et Biophysica Acta (BBA) - Bioenergetics*, 2000, **1458**, 148–163.
8 M. Flores, A. Savitsky, M. L. Paddock, E. C. Abresch, A. A. Dubinskii, M. Y. Okamura, W. Lubitz and K. Möbius, *J. Phys. Chem. B*, 2010, **114**, 16894–16901.
9 A. Aviram and M. A. Ratner, *Chem. Phys. Lett.*, 1974, **29**, 277–283.
10 E. G. Alexov and M. R. Gunner, *Biochemistry*, 1999, **38**, 8253–8270.
11 J.-y. Hasegawa, M. Ishida, H. Nakatsuji, Z. Lu, H. Liu and W. Yang, *J. Phys. Chem. B*, 2003, **107**, 838–847.
12 M. L. Paddock, M. Flores, R. Isaacson, C. Chang, E. C. Abresch, P. Selvaduray and M. Y. Okamura, *Biochemistry*, 2006, **45**, 14032–14042.
13 D. V. Matyushov, *J. Chem. Phys.*, 2013, **139**, 025102.
14 H. B. Gray and J. R. Winkler, *Proc. Natl. Acad. Sci.*, 2005, **102**, 3534–3539.
15 R. A. Marcus and N. Sutin, *Biochim. Biophys. Acta*, 1985, **811**, 265–322.
16 P. F. Barbara, T. J. Meyer and M. A. Ratner, *J. Phys. Chem.*, 1996, **100**, 13148–13168.
17 C. C. Moser, C. C. Page, X. Chen and P. L. Dutton, *J. Biol. Inorg. Chem.*, 1997, **2**, 393–398.
18 D. N. LeBard and D. V. Matyushov, *Phys. Chem. Chem. Phys.*, 2010, **12**, 15335–15348.
19 V. Tipmanee, H. Oberhofer, M. Park, K. S. Kim and J. Blumberger, *J. Am. Chem. Soc.*, 2010, **132**, 17032–17040.
20 M. McCullagh and G. A. Voth, *J. Phys. Chem. B*, 2013, **117**, 4062–4071.
21 A. Cooper, *Prog. Biophys. Molec. Biol.*, 1984, **44**, 181–214.
22 A. Crisanti and F. Ritort, *J. Phys. A: Math. Gen.*, 2003, **36**, R181–290.
23 D. R. Martin and D. V. Matyushov, *J. Chem. Phys.*, 2015, **142**, 161101.
24 D. W. Small, D. V. Matyushov and G. A. Voth, *J. Am. Chem. Soc.*, 2003, **125**, 7470–7478.
25 M. H. B. Stowell, T. M. McPhillips, D. C. Rees, S. M. Soltis, E. Abresch and G. Feher, *Science*, 1997, **276**, 812–816.
26 E. Nabedryk and J. Breton, *Biochimica et Biophysica Acta (BBA) - Bioenergetics*, 2008, **1777**, 1229–1248.
27 B. Rabenstein, G. M. Ullmann and E.-W. Knapp, *Biochemistry*, 2000, **39**, 10487–10496.
28 J. L. Klepeis, K. Lindorff-Larsen, R. O. Dror and D. E. Shaw, *Curr. Opin. Struct. Biol.*, 2009, **19**, 120–127.
29 S. E. Walden and R. A. Wheeler, *J. Phys. Chem. B*, 2002, **106**, 3001–3006.
30 R. A. Kuharski, J. S. Bader, D. Chandler, M. Sprik, M. L. Klein and R. W. Impey, *J. Chem. Phys.*, 1988, **89**, 3248–3257.
31 H. Ito and H. Nakatsuji, *J. Comput. Chem.*, 2001, **22**, 265–272.
32 F. Burggraf and T. Koslowski, *Biochimica et Biophysica Acta (BBA) - Bioenergetics*, 2011, **1807**, 53–58.
33 H. Kitoh-Nishioka and K. Ando, *J. Phys. Chem. B*, 2012, **116**, 12933–12945.
34 R. Calvo, M. C. Passeggi, R. A. Isaacson, M. Y. Okamura and G. Feher, *Biophys. J.*, 1990, **58**, 149–165.
35 N. Leioatts, B. Mertz, K. Martínez-Mayorga, T. D. Romo, M. C. Pitman, S. E. Feller, A. Grossfield and M. F. Brown, *Biochemistry*, 2014, **53**, 376–385.
36 S. Chakrabarty and A. Warshel, *Proteins*, 2013, **81**, 93–106.
37 J. C. Rasaiah, S. Garde and G. Hummer, *Annu. Rev. Phys. Chem.*, 2008, **59**, 713–740.
38 M. D. Collins, G. Hummer, M. L. Quillin, B. W. Matthews and S. M. Gruner, *Proc. Natl. Acad. Sci. USA*, 2005, **102**, 16668–16671.

Physical Chemistry Chemical Physics Accepted Manuscript

39 A. Migliore, N. F. Polizzi, M. J. Therien and D. N. Beratan, *Chem. Rev.*, 2014, **114**, 3381–3465.
40 P. C. Marijuán, *BioSystems*, 1991, **25**, 259–273.
41 J. M. R. Parrondo, J. M. Horowitz and T. Sagawa, *Nat. Phys.*, 2015, **11**, 131–139.
42 D. Bratko, C. D. Daub and A. Luzar, *Phys. Chem. Chem. Phys.*, 2008, **10**, 6807–6813.

Physical Chemistry Chemical Physics Accepted Manuscript

This journal is © The Royal Society of Chemistry [year]